View metadata, citation and similar papers at core.ac.uk
brought to you by CORE
provided by Open Repository and Bibliography - Luxembourg

PHYSICAL REVIEW A **82**, 062902 (2010)

Rumpling of LiF(001) surface from fast atom diffraction

A. Schüller, S. Wethekam, D. Blauth, and H. Winter*
Institut für Physik, Humboldt Universität zu Berlin, D-12489 Berlin, Germany, EU

F. Aigner, N. Simonović,† B. Solleder, and J. Burgdörfer
Institute for Theoretical Physics, Vienna University of Technology, A-1040 Vienna, Austria, EU

L. Wirtz‡
Institute for Electronics, Microelectronics, and Nanotechnology (IEMN), CNRS-UMR 8520, Department ISEN, B.P. 60069, F-59652 Villeneuve d'Ascq Cedex, France, EU

(Received 4 August 2010; published 14 December 2010)

Quantum diffraction of fast atoms scattered from the topmost layer of surfaces under grazing angles of incidence can be employed for the analysis of detailed structural properties of insulator surfaces. From comparison of measured and calculated diffraction patterns we deduce the rumpling of the topmost surface layer of LiF(001) (i.e., an inward shift of Li^+ ions with respect to F^- ions). The effect of thermal vibrations on the measurement of rumpling is accounted for by *ab initio* calculations of the mean-square vibrational amplitudes of surface ions. At room temperature this leads to a reduction of the apparent rumpling by 0.008 Å. We then obtain a rumpling of (0.05 ± 0.04) Å, which improves its accuracy achieved in previous work.

DOI: 10.1103/PhysRevA.82.062902 PACS number(s): 79.20.Rf, 34.20.−b, 68.49.Bc, 68.35.B−

I. INTRODUCTION

Diffraction effects for particles is a spectacular manifestation of quantum physics which has been observed for objects as heavy as fullerenes [1]. In surface science, starting with the pioneering work by Estermann and Stern [2], slow ("thermal") helium atom scattering, where the wavelength of matter waves associated with the motion of atoms is comparable to interatomic distances in the topmost surface layer, has become a versatile and powerful analytical tool [3,4]. Recently, quantum diffraction was also observed for fast, energetic (up to several keV) atoms scattered under grazing angles of incidence along low indexed atomic strings of the topmost surface layer [5–8] in terms of "axial surface channeling" [9].

For fast atoms, the de Broglie wavelength associated with matter waves is about three orders of magnitude smaller than typical interatomic spacings in crystal lattices and smaller than thermal vibration amplitudes of surface atoms with a multitude of open reaction and excitation channels at these projectile energies. Thus, one might expect the coherence in the scattering process to be effectively destroyed. However, electronic excitations owing to the wide-band gap of LiF and inelastic phonon excitations are sufficiently suppressed for quantum diffraction to persist [5–8,10,11].

In this work, fast atom diffraction (FAD) is used to derive fine details of the surface structure with unprecedented accuracy. We focus on the prominent case of slight deviations of the stable (001) face of an LiF crystal surface from the ideal coplanar square checkerboard lattice with alternating Li^+ and F^- ions on adjacent lattice positions. These displacements between the equilibrium positions of the different ion species normal to the surface plane, called "rumpling" or "buckling" δz, result from the polarization of the ions of the surface in the electrostatic field of the ions of the bulk [12–14]. Since the polarizabilities of anions and cations are different, the induced dipole moments lead to a different relaxation of the F^- sublattice with respect to the Li^+ sublattice in the topmost layer of LiF(001).

For this simple lattice arrangement, which makes the topmost layers of the LiF(001) surface a model system for the surface structure of ionic crystals, the position of atoms in the topmost layers is far from being accurately known. Early studies using low-energy electron diffraction (LEED) based on the analysis of experimental diffraction spot intensities versus electron energy [I(V)-curves] indicated a displacement of the Li^+ ions relative to the F^- ions by 0.25 Å toward the bulk [15]. The evaluation of data obtained via thermal energy atom scattering with He atoms (HAS) concluded a shift of (0.036 ± 0.006) Å in the opposite direction (i.e., from the bulk toward vacuum [16,17]). Recently, a fully dynamical LEED analysis of I(V) curves for thin LiF(001) films grown on Pt(111) deduced a shift of the Li^+ ions by (0.24 ± 0.04) Å toward the bulk [18], whereas similar studies using a single crystal (001) surface report a displacement of (0.04 ± 0.20) Å only [19,20]. The latter value is in good agreement with recent calculations based on Hartree-Fock theory [11] and on density functional theory (DFT) [21–23] but has a considerable uncertainty.

FAD interference patterns show a pronounced sensitivity on the projectile-surface interaction potential which results from the specific interatomic potentials depending on the positions of the surface atoms. Based on DFT, we have performed first principle calculations on the interaction potential for He atoms in front of LiF(001) for given rumplings δz. These potentials serve as input for wave-packet simulations of the scattering process in order to deduce δz from best fits to experimental diffraction patterns.

*winter@physik.hu-berlin.de
†Present address: Institute of Physics, P.O. Box 57, 11001 Belgrade, Serbia.
‡ludger.wirtz@isen.iemn.univ-lille1.fr

 ©2010 The American Physical Society

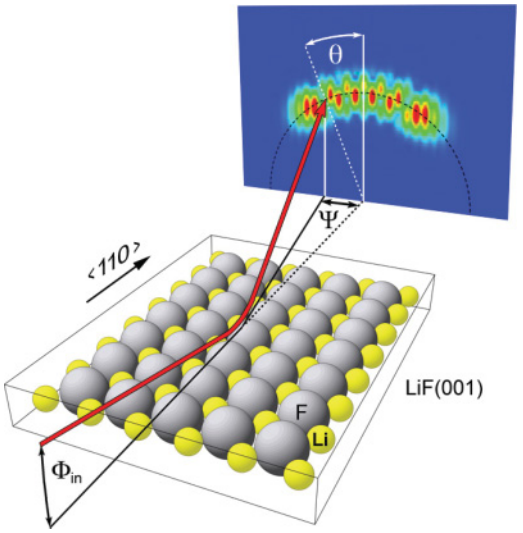

FIG. 1. (Color online) Sketch for scattering of fast atoms from the LiF(001) surface under the grazing angle of incidence Φ_{in} along a ⟨110⟩ direction.

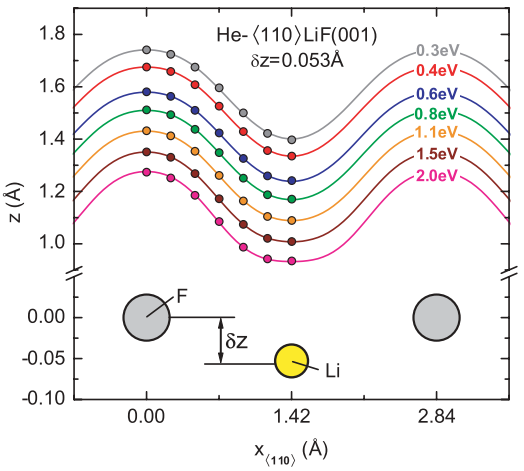

FIG. 2. (Color online) Equipotential lines of potential between the He atom and LiF(001) surface averaged along strings of Li^+ and F^- ions of a ⟨110⟩ direction. δz, vertical displacement between F^- and Li^+ in the topmost surface layer, so-called "rumpling".

II. EXPERIMENTAL METHOD AND OBSERVATIONS

A. Experimental setup and interaction scenario

In our experiments, He atoms with kinetic energies E_0 of about 300 eV to 3 keV were scattered from a clean and flat LiF(001) surface at room temperature under fixed grazing angles of incidence Φ_{in} ranging from about 0.5° to 1.5°. A ⟨110⟩ direction in the (001) plane was aligned along the direction of the incident projectile beam so that scattering proceeds along channels formed by alternating strings of Li^+ and F^- ions in the topmost surface layer. A sketch of the scattering geometry is shown in Fig. 1. The collision with the surface proceeds in the regime of "axial surface channeling" where the motions of projectiles parallel and normal to the channels are widely decoupled in terms of a "fast" parallel motion with energy $E_\parallel = E_0 \cos^2 \Phi_{in}$ and a "slow" normal motion with energy $E_\perp = E_0 \sin^2 \Phi_{in}$. Then the effective potential of the projectile atom in front of the surface results from averaging of the interaction potential along strings formed by lattice atoms [9,24]. The effective (averaged) interaction potential for He atoms scattered along ⟨110⟩ direction is shown in Fig. 2 in a plane normal to the atomic strings. The contour lines denote equipotential planes from 0.3 eV to 2.0 eV obtained from our DFT calculations showing a pronounced corrugation with a maximum on top of strings formed by F^- ions and a minimum on top of Li^+ strings. This corrugation is significantly enhanced by the rumpling δz resulting in a pronounced effect on the observed diffraction patterns.

The beam of fast He atoms was produced by neutralization of He^+ ions from an accelerator with a 10-GHz electron cyclotron resonance (ECR) ion source (Nanogan, Pantechnique, France). The neutralization of the He^+ ions was achieved via charge transfer in a gas cell mounted in the beam line operated with He gas. Residual ions were removed by an electric field. A base pressure of some 10^{-11} mbar was achieved in our UHV chamber by a turbomolecular pump in a series with a titanium sublimation pump. The pressure gradient with respect to the beam line was maintained by two differential pumping stages. Two pairs of orthogonal slits of 0.2-mm widths which are separated by 740 mm were used for the collimation of the incident beam to a divergence of less than 0.03°. Such a high angular collimation is needed for resolving discrete diffraction spots.

The LiF(001) surface was prepared by cycles of grazing sputtering with 25 keV Ar^+ ions at 250 °C (where the ionic conductivity of LiF is sufficiently enhanced) and subsequent annealing to temperatures of about 350 °C.

B. Diffraction patterns

Angular distributions for scattered projectiles were recorded 66 cm behind the target by means of a position sensitive microchannel plate detector [25]. With a flux of incident neutral atoms lower than 10^4 s^{-1} probing a surface area of about 1 mm^2, diffraction patterns can be recorded in times of typically some seconds to minutes. Under these conditions, radiation damage of the target surface as well as charging effects are completely negligible. In contrast to available standard surface analytical tools, such as, for example, low-energy electron diffraction (LEED), this technique can therefore be applied in studies on surfaces of insulator crystal targets at room temperature and surface structures sensitive to electron or photon irradiation.

As representative examples, we present in Fig. 3 diffraction patterns as recorded with the position-sensitive detector for scattering of 0.65, 0.85, and 1.0 keV ^3He atoms from LiF(001) under $\Phi_{in} = 0.99°$ along a ⟨110⟩ channel. The well-defined diffraction spots are positioned on a circle of radius Φ_{in} owing to energy conservation of the normal motion for elastic scattering from strings under axial symmetry (see circle in the detector plane in Fig. 1). With increasing energy E_0 (decreasing de Broglie wavelength with respect to normal motion $\lambda_{dB\perp}$) the relative intensity of diffraction spots changes. At $E_0 = 0.65$ keV (top panel) the zeroth-order spot $n = 0$ in the center of the distribution at $\Psi = 0$ is very weak, whereas the adjacent first-order diffraction spot $n = 1$ is intense. At

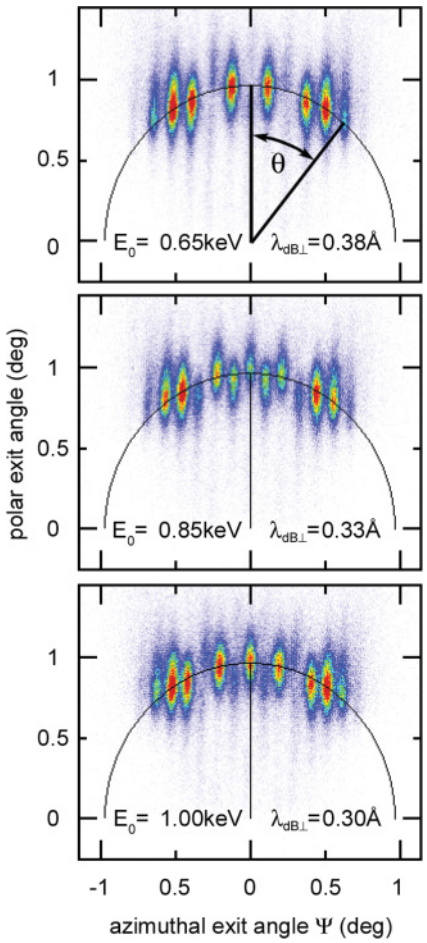

FIG. 3. (Color online) Diffraction pattern as recorded with position-sensitive channel plate detector for ^{3}He atoms scattered from the LiF(001) surface along ⟨110⟩ under $\Phi_{in} = 0.99^\circ$ with energies of 0.65 keV (top panel), 0.85 keV (middle panel), and 1.00 keV (bottom panel). Color code is as follows: red (dark gray) indicates high intensity, light blue (light gray) indicates low intensity. Circle of radius Φ_{in} indicates positions for elastic scattering.

$E_0 = 0.85$ keV (middle panel) both spots are present and at $E_0 = 1.00$ keV (bottom panel) $n = 0$ is intense whereas $n = 1$ is weak.

These features are most clearly present in Fig. 4, where we show projections of the intensities for a narrow interval of angles centered around circles of radius Φ_{in} as a function of the deflection angle Θ. The contributions of the zeroth- and first-order diffraction spots are highlighted. Θ is related to the azimuthal exit angle Ψ (cf. Fig. 1) via the relation $\Theta = \arcsin(\Psi/\Phi_{in})$.

The quantum diffraction patterns can be attributed to scattering from axial atomic strings oriented parallel to the incident beam and separated by a distance d [5–7]. The angular positions of diffraction spots of order n follow from the Bragg condition $d \sin\Psi = n\lambda_{dB}$. This is equivalent to $d \sin\Theta = n\lambda_{dB\perp}$ where $\lambda_{dB\perp} = \lambda_{dB}/\sin\Phi_{in} = h/(2ME_\perp)^{1/2}$ is the de Broglie wavelength attributed to the motion of projectiles normal to axial strings (h = Planck's constant; M = mass of the projectile). For grazing angles of incidence of typically $\Phi_{in} = 1^\circ$, $\lambda_{dB\perp}$ is about two orders of magnitude

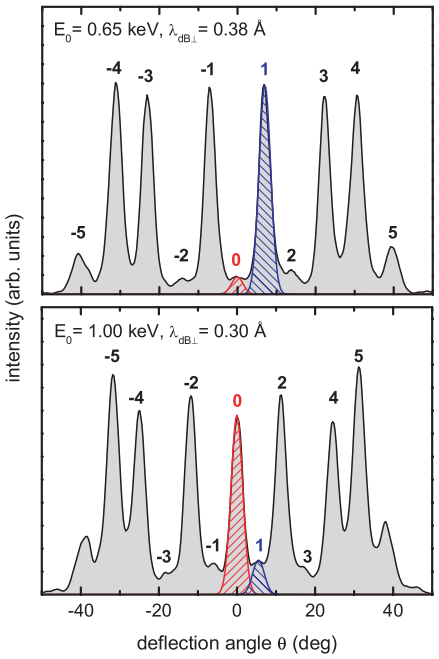

FIG. 4. (Color online) Intensity within a narrow interval of angles centered around the circle of radius Φ_{in} in Fig. 3 as a function of the deflection angle Θ. Numbers denote diffraction order n with $n = 0$ being highlighted in red (center) and $n = 1$ in blue (just right of center).

larger than λ_{dB} associated with the total projectile energy and hence comparable to interatomic spacings of the crystal lattice. The zeroth-order spot ($n = 0$) is located in the center ($\Psi = \Theta = 0$), while higher orders appear symmetrically on both sides for nonzero Ψ or Θ. A striking feature of the angular distributions as shown in Figs. 3 and 4 is a change of relative spot intensities for a given diffraction order as a function of $\lambda_{dB\perp}$. This change can be understood in terms of "supernumerary rainbows" [7,26,27] and has its origin in the corrugation of the interaction potential [6,7,11,22,28] which depends on the rumpling.

In order to investigate the intensity modulations of diffraction spots as a function of $\lambda_{dB\perp}$ in more detail, we have constructed *diffraction charts* by combining projections as shown in Fig. 4 for a series of normal de Broglie wavelengths $\lambda_{dB\perp}$. In Fig. 5, we show the intensity of diffraction patterns as a function of $\lambda_{dB\perp}$ and Θ as "three-dimensional" plots of experimental intensity distributions for the scattering of ^{3}He atoms from LiF(001) along a ⟨110⟩ direction. This plot is generated from projections of 52 different intensity distributions as shown in Fig. 4. For illustration, we have highlighted the two projections from Fig. 4 by black curves in the top panel. For comparison of experiment with calculations, such diffraction charts contain complete information on the diffraction scenario. One important advantage of those charts is their detailed information on the modulation structure over the relevant diffraction orders. Another is the better control of decoherence as compared to the individual diffraction pattern (such as Fig. 3; see [11]). The positions of diffraction spots of order n are determined by the periodicity of the interaction potential and result from the Bragg condition $\Theta_n = \arcsin(n\lambda_{dB\perp}/d)$ while the positions of intensity maxima and

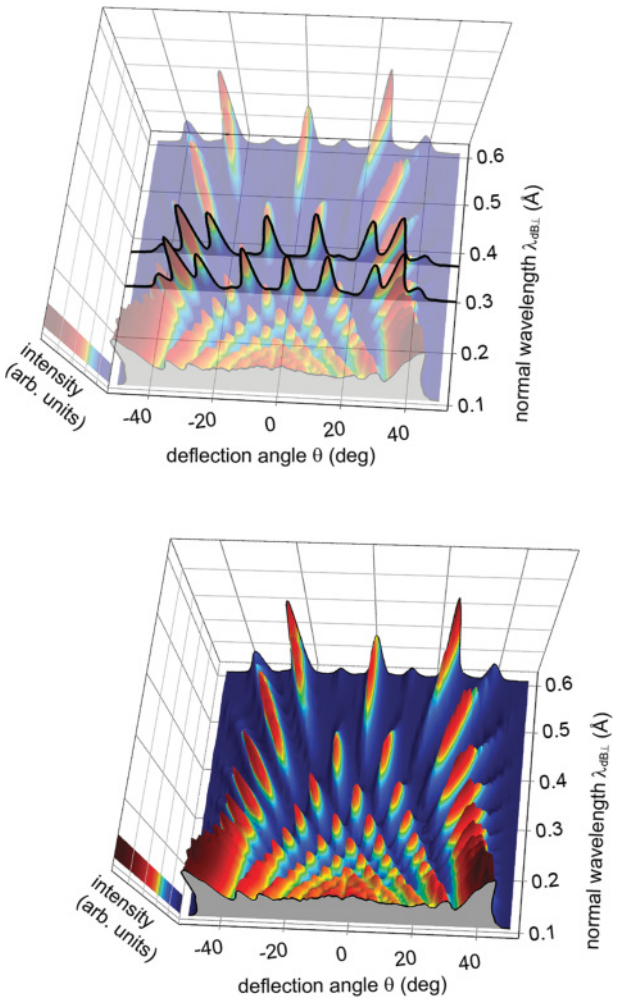

FIG. 5. (Color online) Three-dimensional plots of experimentally deduced intensities as function of deflection angle Θ and normal de Broglie wavelength $\lambda_{dB\perp}$ for scattering of ^{3}He atoms from LiF(001) along a ⟨110⟩ direction. Projections of intensity distributions as shown in Fig. 4 are highlighted as black curves in upper panel. The same data are shown as two-dimensional diffraction chart in Fig. 8.

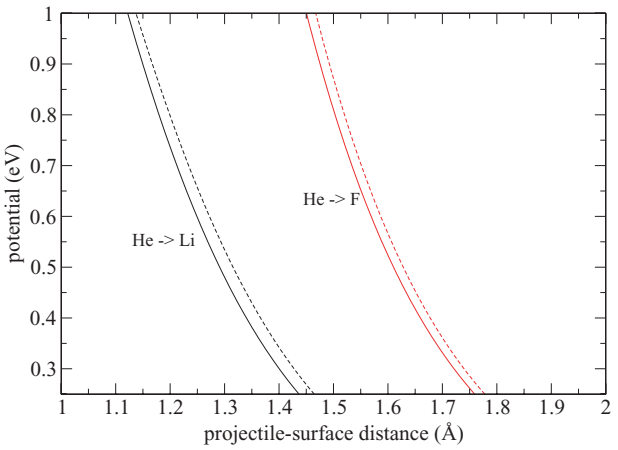

FIG. 6. (Color online) Interaction potential, averaged along a ⟨110⟩ direction, between a He projectile and a LiF surface as a function of the distance z to surface. Left solid curve, incidence on top of Li ions; right solid curve, incidence on top of F ions; dashed curves, potentials including an average over thermal displacements (see text).

minima of given order n result from the corrugation of the effective potential (cf. Fig. 2). The peak at maximum angular deflection is the so-called "quantum surface rainbow" [26] in close analogy to the classical rainbow [29] while maxima at smaller deflection angles belong to different supernumerary rainbows as discussed in Ref. [22]. From the comparison of diffraction charts from experiments with simulations we deduce the rumpling of LiF(001) as outlined below.

III. THEORETICAL MODEL

A. Interaction potential

The interaction potential between the He projectile and the LiF surface was calculated with density-functional theory (DFT) in the local density approximation (LDA) using the code ABINIT [30]. The system is represented by a supercell, comprising the projectile and a LiF slab that represents the surface. By implementing supercells of different sizes, we checked carefully that it is sufficient to use a two-layer slab with an interslab vacuum of 7.5 Å and to represent the surface by its primitive cell. This entails a periodic array of He atoms with nearest-neighbor distance of 2.84 Å colliding with the surface. However, due to the noble gas electronic configuration, He atoms in neighboring supercells do not interact with each other [31]. Wave functions were expanded in plane waves with an energy cutoff at 40 hartree. Core electrons were replaced by pseudopotentials of the Troullier-Martins type [32]. The interaction potential was obtained as the total energy of the combined system (slab + He) minus the sum of the total energies of the slab and of the He atom, an example of which is shown in Fig. 2, averaged along a ⟨110⟩ direction (cf. Fig. 1). The curves represent the interpolation between the calculated points (circles), which serves as input for our wave-packet simulations. The key parameter in the simulation of the diffraction pattern is the full corrugation Δz (i.e., the normal distance between the minimum of an equipotential line above the string of Li^+ ions and the maximum above the F^- ions). In Fig. 6, we show the potential averaged along a ⟨110⟩ direction for the He atom on top of a string of F^- ions and a string of Li^+ ions (solid curves). The two curves are almost parallel (i.e., the corrugation Δz as function of the potential energy is almost constant). For energies larger than 0.3 eV the corrugation Δz is in accord with results from DFT calculations by Pruneda reported in Ref. [22] as well as the potential from Hartree-Fock calculations used in Ref. [11]. The latter was extrapolated to the region of limited computational accuracy (energies smaller than 0.5 eV) under the constraint of Δz remaining constant in order to achieve good agreement with the experiment. For energies lower than 0.3 eV, the corrugation in the three calculations (Refs. [11,22]; this work) differs [33]. Therefore, we consider in our analysis of the rumpling diffraction patterns for energies $E_\perp > 0.3$ eV only.

The corrugation of the potential depends sensitively on the rumpling of the surface. Furthermore, it may be affected by the thermal displacements of the surface ions, in particular,

when the vibrational amplitudes of the lighter Li^+ ions are considerably larger than the vibrational amplitudes of the heavier F^- ions. Rumpling and vibrational amplitudes have therefore to be discussed in detail.

B. Surface rumpling and effect of thermal displacements

In order to scrutinize the reliability of our DFT-LDA calculation of surface rumpling and thermal vibration amplitudes, we checked if the phonon dispersion relation of bulk LiF is adequately reproduced.

1. Phonons of bulk LiF

The vibronic structure of bulk LiF was calculated using density-functional perturbation theory (DFPT) [34,35] implemented in the code ABINIT [30]. The plane wave energy cutoff was set to 100 hartree and we carefully checked the convergence of the Li pseudopotential (using a cutoff radius of 0.5 a.u.), explicitly including the Li 1*s* electrons as valence electrons [36]. Geometry optimization (energy minimization) yielded a lattice constant of 7.428 a.u. (slightly smaller than the experimental value 7.6 a.u.). We used the optimized lattice constant for the phonon calculations. The resulting bulk phonon dispersion relation [Fig. 7(a)] is in excellent agreement with the measured phonon dispersion [37], only the frequencies of the transverse optical (TO) mode are slightly overestimated in our calculations. In Fig. 7(b) we show the phonon dispersion relation of a five-layer slab of LiF. The lowest acoustic mode is the Rayleigh mode (which is localized at the surface). It compares reasonably well with experimental data [38–40] along the directions $\bar{\Gamma} \rightarrow \bar{M}$ and $\bar{\Gamma} \rightarrow \bar{X}$. We conclude that DFT-LDA is sufficiently reliable to calculate the forces between lattice ions of LiF. Thus we expect an adequate description of the surface rumpling and the amplitudes of thermal vibrations for LiF.

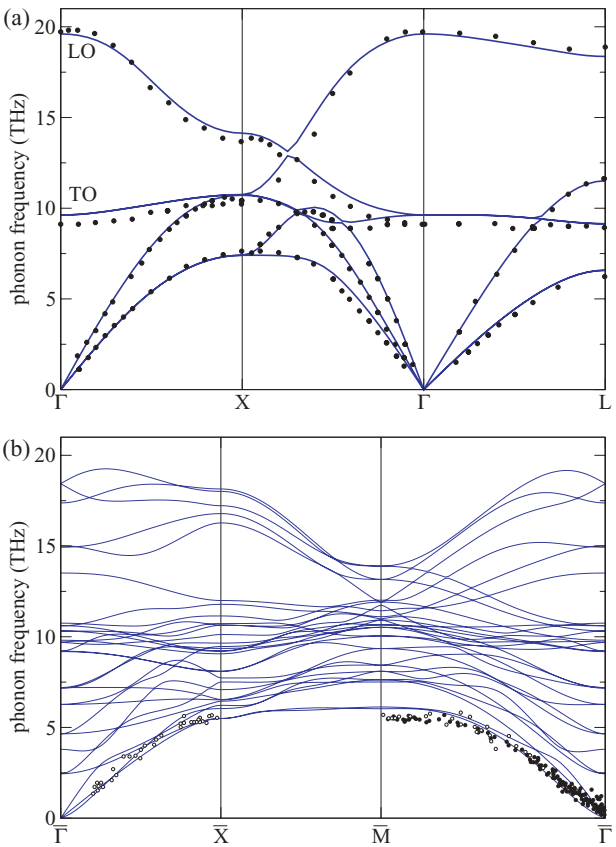

FIG. 7. (Color online) (a) Phonon dispersion relation of bulk LiF. Solid lines, our *ab initio* calculations; circles, neutron diffraction data ($T = 295$ K) from Ref. [37]. (b) Phonon dispersion relation of a five-layer LiF slab. Circles, measurement of the Rayleigh mode by high-resolution helium time-of-flight studies from Ref. [38] (solid circles) and Ref. [39] (open circles).

2. Surface rumpling

In order to determine the relaxation of surface ions, we used a five-layer slab with the optimized bulk lattice constant. Geometry optimization yielded a surface rumpling of $\delta z = 0.057$ Å with the F^- ions displaced outward and the Li^+ ions displaced inward. This is in reasonable agreement with earlier DFT calculations ($\delta z = 0.06$ Å using LDA and a Gaussian orbital basis [21], $\delta z = 0.068$ Å based on the generalized-gradient approximation (GGA) [23], and $\delta z = 0.049$ Å from LDA [22]). Indeed, the differences between the calculations are a measure for the uncertainties inherent in the DFT calculations which depend on the exchange-correlation functional: LDA tends to overbind (underestimate of bond lengths and thus also of rumpling) and GGA tends to underbind (overestimate of the bond lengths and the rumpling) [41]. Our calculated surface rumpling is also close to the value of 0.062 Å, obtained by de Wette *et al.* with the semiempirical shell model [13] (which was parameterized to yield good agreement for the bulk phonon dispersion relation).

3. Root-mean-square vibrational amplitudes

From the phonon frequencies $\omega_n(\vec{k})$ (n denoting the phonon branch) and the normalized phonon eigenvectors $e_{n,\alpha,i}(\vec{k})$, we derive the mean-square vibrational amplitude (MSVA) of atom α in direction i [42]:

$$\langle u^2_{\alpha,i} \rangle = \frac{\hbar}{2M_\alpha} \sum_{n=1} \int d^3k \frac{1}{\omega_n(\vec{k})} |e_{n,\alpha,i}(\vec{k})|^2 \coth \left[\frac{\hbar \omega_n(\vec{k})}{2k_B T} \right]. \quad (1)$$

The integral is performed over all wave vectors in the first Brillouin zone. For bulk LiF at $T = 300$ K we obtain $\langle u^2_{\mathrm{Li}} \rangle = 0.0118$ Å^2 and $\langle u^2_{\mathrm{F}} \rangle = 0.0081$ Å^2 which is very close to the values of Gupta [42], obtained with the semiempirical shell model for the phonons: $\langle u^2_{\mathrm{Li}} \rangle = 0.0116$ Å^2 and $\langle u^2_{\mathrm{F}} \rangle = 0.0079$ Å^2.

In order to evaluate the MSVA of surface ions, we have calculated the phonons of the same five-layer slab of LiF that has been used for the calculation of the surface rumpling. For the surface ions we find vertical vibration amplitudes: $\langle u^2_{\mathrm{Li},\perp} \rangle = 0.0135$ Å^2 and $\langle u^2_{\mathrm{F},\perp} \rangle = 0.0097$ Å^2 which are increased by about 20% compared to bulk vibration amplitudes. The corresponding root-mean-square vibrational amplitudes (RMSVA) at the surface are 0.116 Å for Li^+ ions and 0.098 Å for the F^- ions. These values are about twice as large as the value for the surface rumpling. One may thus wonder if the thermal vibrations partially cancel the effect

of the surface rumpling on the corrugation of the He-LiF interaction potential.

C. Influence of thermal vibrations on the interaction potential

In order to estimate the effect of thermal vibrations on the He-LiF interaction potential, we have calculated the interaction potential $\bar{V}(z)$, averaged over 10 000 different positions of the surface ions. Each ion is individually and randomly displaced such that on average it follows a Gaussian distribution with the full width at half maximum (FWHM) given by the respective RMSVA presented in Sec. III B 3. This corresponds to an uncorrelated motion of neighboring ions. We have used a fit of the *ab initio* potential surface data to analytic functions [43].

In Fig. 6, $\bar{V}(z)$ is compared to the potential $V_0(z)$, the potential at the average position of the surface ions. Clearly, $\bar{V}(z)$ is shifted outward with respect to $V_0(z)$. In the energy interval between 0.25 and 0.8 eV (the interval of interest for our scattering experiments), the offset between $\bar{V}(z)$ and $V_0(z)$ is almost energy independent: $\bar{V}(z) = V_0(z - \Delta)$. The outward shift is slightly larger on top of the Li-ion chain than on top of the F-ion chain: $\Delta_{Li} = 0.025$ Å and $\Delta_F = 0.017$ Å. This introduces an additional "thermal corrugation" of the potential with amplitude $\Delta_F - \Delta_{Li} = -0.008$ Å. This is about 14% of the calculated geometric rumpling. Since its sign is negative, it reduces the effect of geometric rumpling on the potential corrugation.

D. Wave-packet simulation of atom-surface scattering

Our scattering analysis is based on the solution of the stochastic Schrödinger equation for a wave packet scattered from the LiF(001) surface, taking into account collisionally induced decoherence within the framework of an open quantum system (OQS) approach in terms of random momentum transfers [44]. While violent collisions lead to electronic excitations and ionization, soft collisions result in momentum and energy exchange with the surface, namely the excitation of optical and acoustic phonons, giving rise to angular spread and, concomitantly, to random phases for the evolution of the wave packet and thus decoherence. Propagation of the wave packet proceeds in the two-dimensional landscape of the axial channeling potential,

$$V(y,z) = \frac{1}{L}\int_{x_0}^{x_0+L} dx\, V(x,y,z), \tag{2}$$

using as input the full three-dimensional surface potential discussed in Sec. III A. We assume that the free motion along the surface ($\hat{x}$) and in the transverse plane (y,z) are approximately decoupled from each other. However, the stochastic momentum transfers account, to first order, for coupling between these degrees of freedom.

Accordingly, we use the split-operator fast Fourier transform (FFT) method [45] for calculating the propagation of the normal component. Neglecting the initial incoherent beam divergence, the incident wave packet has the form,

$$\Psi_{\rm in}(\vec{r}) = e^{ik_\parallel x}\Psi_\perp(y,z). \tag{3}$$

The normal component is taken in the form of the Gaussian wave packet,

$$\Psi_\perp(x,y) \propto e^{-ik_\perp z} e^{-y^2/2\sigma_y^2} e^{-(z-z_0)^2/2\sigma_z^2}, \tag{4}$$

where $k_{\parallel,\perp} = 2\pi/\lambda_{{\rm dB}\parallel,\perp} = (2ME_{\parallel,\perp})^{1/2}/\hbar$ are the parallel (normal) components of the incident particle wave vector $\mathbf{k}$. Here, $\sigma_{y,z}$ are equal to the transverse coherence length of the incident beam. The transverse coherence length is large compared to the lattice spacing. In fact, Eq. (4) is close to a delocalized plane wave. The effect of decohering interactions with the surface results in a drastic reduction of the transverse coherence length along the polar angle, $\sigma_z^{\rm out} \ll \sigma_z^{\rm in}$, and thus a localization of the transverse wave packet in the z direction [11]. However, since the diffraction charts introduced in Sec. II B are less affected by incoherent beam broadening and reduction of transverse coherence length than individual diffraction images at a fixed $\lambda_{\rm dB}$, these charts can be approximately reconstructed using the initial wave packets $\Psi_\perp$ with a very large σ_y and almost any value for σ_z provided that the initial wave packet does not overlap with the surface. In the special case when $\sigma_y \to \infty$ the wave packet (4) reduces to a plane wave modulated in the z direction only [i.e., $\Psi_\perp(y,z) \propto e^{-ik_\perp z} e^{-(z-z_0)^2/2\sigma_z^2}$]. In this case, making use of the periodicity of the averaged potential, the calculation can be performed in the grid area restricted to a single lattice period (or few of them) of the averaged potential.

For extracting the probability distribution of the scattered wave in the asymptotic region it is convenient to use the momentum representation of wave function (the distribution $|\Psi_\perp^{\rm out}(k_y,k_z)|^2$ reproduces the interference pattern). Since the application of the evolution operator in the method used here is based on the transformations from the coordinate to the momentum representation and *vice versa* (by use of the FFT procedure; see Ref. [45]), this method automatically provides the wave function in both representations.

In Fig. 8, we compare diffraction charts from the experiments with those from wave-packet simulations for scattering of ^{3}He atoms along a ⟨110⟩ direction. Since the charts are symmetric with respect to Θ, we have plotted for a better

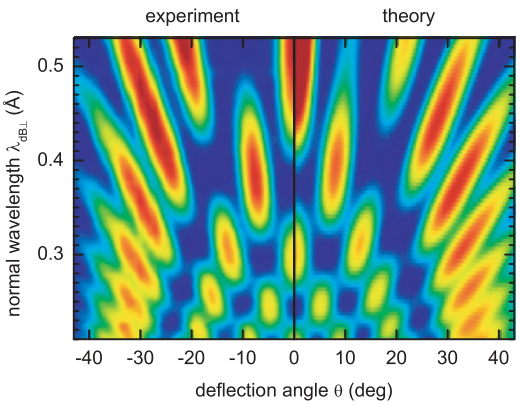

FIG. 8. (Color online) "Diffraction charts" constructed from a series of diffraction patterns for scattering of ^{3}He atoms from LiF(001) along a ⟨110⟩ direction. Experimental data (left) are in accord with theoretical results from wave-packet simulations taking into account a rumpling of $\delta z = 0.05$ Å (right). Red (dark oval shapes), high intensity; blue (background), low intensity.

comparison the experimental data in the left half of the chart and the calculated pattern in the right part only. The experimental data are the same as shown in Fig. 5. The position of intensity maxima and minima of all diffraction orders as well as the intensity distribution are well reproduced by the wave-packet simulation if rumpling is taken into account.

IV. EXTRACTION OF SURFACE RUMPLING

In Fig. 9, the relative intensities of the diffraction orders $n = 0$ (top panel) and $n = 1$ (bottom panel) are plotted as a function of $E_\perp = h^2/(\lambda_{\mathrm{dB}\perp}^2 2M)$. This corresponds to a cut in the diffraction chart in Fig. 8 at $\Theta = 0$ and $\Theta = \arcsin \lambda_{\mathrm{dB}\perp}/d$, respectively. Since the corrugation of the present *ab initio* potential (if $\delta z = 0.049$ Å is chosen) is in agreement with the *ab initio* calculation from Pruneda [22] at $V > 0.3$ eV only, we consider data with normal energies $E_\perp > 0.3$ eV. The relative intensity for $n = 0$ shows a maximum, when $n = 1$ exhibits a minimum, and vice versa (cf. also blue and red area in Fig. 4). The positions of the maxima and minima depend (via the interaction potential) on the rumpling δz. For comparison with our experimental data, we have calculated the He-LiF(001) interaction potential for 11 different rumpling values $0 < \delta z < 0.1$ Å and performed the corresponding wave-packet simulations. The simulations taking into account a rumpling of $\delta z = 0.042$ Å (solid curve in Fig. 9) are in good accord with the experimental data (gray symbols). The deviation in the heights of the minima might result from the increase of an incoherent background (offset) due to decoherence processes resulting from electronic excitations which become more probable with increasing energy or angle of incidence [46]. The dash-dotted curve results from a simulation without rumpling. The maxima and minima are shifted to larger $E_\perp$ compared to the experimental data. The negative rumpling of $\delta z = -0.036$ Å as deduced by Garcia [16,17] would result in an even stronger deviation. The dashed curve results from a simulation taking into account a rumpling twice as large ($\delta z = 0.084$ Å). This curve is shifted to smaller $E_\perp$. A larger rumpling as deduced by Roberts *et al.* ($\delta z = 0.24$ Å) [18] or Laramore and Switendick ($\delta z = 0.25$ Å) [15] would result in an even more pronounced offset from the experiment.

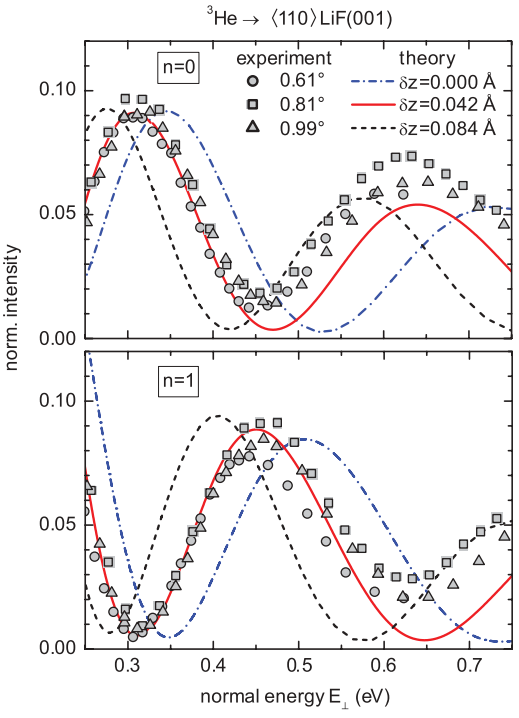

FIG. 9. (Color online) Normalized relative intensity of diffraction order $n = 0$ (top) and $n = 1$ (bottom) for scattering of ^{3}He atoms from LiF(001) along a ⟨110⟩ direction under angle of incidence $\Phi_{\mathrm{in}} = 0.61°$ (circles), 0.81° (squares), 0.99° (triangles) as a function of normal energy $E_\perp$. (Curves) Wave-packet simulations based on He-LiF(001) interaction potential taking into account no rumpling (dash-dotted), a rumpling of $\delta z = 0.042$ Å (solid curve), and $\delta z = 0.084$ Å (dashed).

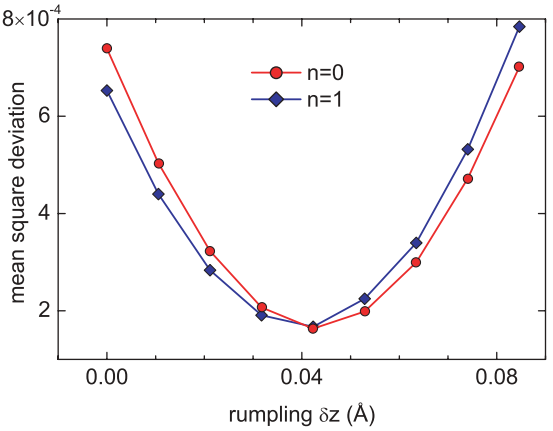

FIG. 10. (Color online) Mean-square deviation of measured and calculated relative intensities of diffraction order $n = 0$ (circles) and $n = 1$ (diamonds) as shown in Fig. 9 as a function of rumpling δz.

Figure 10 shows the mean-square deviation $\sum_{i=1}^{N} (I_i^{\mathrm{exp}} - I_i^{\mathrm{calc}})^2/N$ between experimental and calculated relative intensities of diffraction order $n = 0$ (circles) and $n = 1$ (diamonds) as shown in Fig. 9 as a function of rumpling δz. The best agreement with the experiment is found for a rumpling of $\delta z = 0.042$ Å. Taking into account the reduction of the effect of geometric rumpling on the potential corrugation by the "thermal corrugation," the actual rumpling is $\delta z = (0.042 + 0.008)$ Å $= 0.05$ Å. A conservative estimate of the experimental uncertainty is 0.015 Å. A change of δz by this value results in an increase of the mean-square deviation by almost 50%. The uncertainty of the total energy and energy width of the incident beam is negligibly small. Since the relative intensities at given normal energy is similar for different angles of incidence (symbols in Fig. 9) the uncertainty due to the angular spread contributes only slightly to the uncertainty of δz. A similar experiment analyzed with the same DFT potential will yield a comparable result, but small changes in the theoretical potential can result in a shift of the minimum in Fig. 10. This depends sensitively on the choice of the approximation made for the calculation (e.g., Hartree-Fock or DFT). Within DFT, the result depends on the choice of the exchange-correlation functional (i.e., LDA, GGA, hybrid functionals). Furthermore, the choice of the basis set, energy cutoff, and pseudopotential functions [47] can influence the corrugation. An estimation based on different parameter choices results in an uncertainty of ± 0.03 Å.

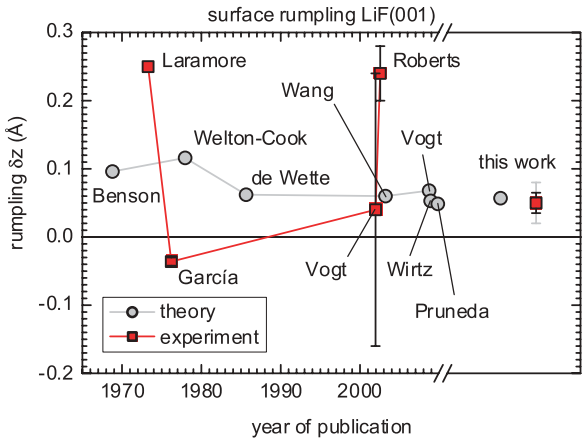

FIG. 11. (Color online) Surface rumpling of LiF(001). (Squares) Experimental values deduced by LEED from Laramore and Switendick [15], Vogt and Weiss [19,20], and Roberts *et al.* [18], by HAS from Garcia [16], and by FAD from this work (black error bar, uncertainty based on present interaction potential; gray error bar, estimation on possible results with other interaction potentials from different approximations within the DFT). (Circles) Theoretical values from shell-model calculations from Benson and Claxton [14], Welton-Cook and Prutton [12], and de Wette *et al.* [13], from Hartree-Fock calculations by Wirtz reported in Ref. [11], and from DFT calculations by Wang *et al.* [21], Vogt [23], Pruneda reported in Ref. [22], and Wirtz (this work).

In Fig. 11, we compare theoretical (circles) and experimental (squares) rumpling values from literature with the rumpling derived in this work. The black error bar represents the experimental uncertainty from the analysis based on the present DFT interaction potential. The gray error bar symbolizes our estimate on possible results in the analysis of experimental data based on other interaction potentials from calculation using different established approximations within the DFT. Our final result of $\delta z = (0.05 \pm 0.04)$ Å is in good agreement with our DFT calculation of $\delta z = 0.057$ Å and the DFT calculations from Wang *et al.* [21], Vogt [23], and Pruneda reported in Ref. [22]. The result from an I(V)-LEED analysis by Vogt and Weiss [19,20] ($\delta z = 0.04 \pm 0.2$ Å) is in accord with our work, but has a larger uncertainty. The analysis of experimental data by Garcia [16,17], Laramore and Switendick [15], and Roberts *et al.* [18] are in conflict with our result. The analysis of thermal helium scattering by Garcia is based on a "hard wall approximation" [16,17]. The evaluation relies on a touching hard sphere model, which is a rather crude model. Thus, the resulting negative rumpling value might result from a poor description of the interaction potential. Laramore and Switendick [15] did not provide error bars. Since a significantly wider data range has been investigated in the experiments by Vogt and Weiss [19], we consider the latter as more reliable. Roberts *et al.* [18] performed an analysis of I(V)-LEED curves similar to the I(V)-LEED curves from Vogt and Weiss [19], but obtained a larger rumpling. A possible reason for this anomalous large value is ascribed to a reduction of the ionic radii at surface. DFT calculations, however, do not provide an indication for such an effect [23].

V. SUMMARY AND CONCLUSIONS

Fast atom diffraction is applied to study the surface rumpling of LiF(001) in the topmost surface layer (i.e., a contraction of Li^+ ions toward the bulk compared to F^- ions). From a comparison of experimental diffraction charts with wave-packet simulations based on *ab initio* interaction potentials for different rumpling values taking into account the effect of thermal vibrations of surface atoms, we deduce $\delta z = (0.05 \pm 0.04)$ Å. This value is in good agreement with our DFT calculations with $\delta z = 0.057$ Å and is more accurate than previous experimental results. The accuracy of the *ab initio* calculations for the potential surfaces is, however, limited by the approximations used (DFT-LDA). Future theoretical work may improve the accuracy of the interaction potential [47] and result in a reduced uncertainty for the deduced rumpling. The major theoretical advance of this paper with respect to previous results consists in the detailed analysis of the influence of the thermal vibrations on the corrugation of the potential. We performed *ab initio* calculations of the root-mean-square vibrational amplitudes of the surface ions and obtained 0.116 Å for Li^+ ions and 0.098 Å for the F^- ions. Performing a thermal average of the potential surfaces with these vibrational amplitudes leads to a "thermal" contribution to the potential corrugation of −0.008 Å.

The remarkable spatial resolution of the highly surface-sensitive FAD method bears the potential for a versatile surface-analytical tool, whenever decoherent processes in fast atomic surface scattering are sufficiently suppressed [11]. This feature was demonstrated in studies on insulator [5,6] and semiconductor [48,49] surfaces with direct band gap. Recent work demonstrates that such a regime is also met for scattering from clean [50,51] and adsorbate covered [52,53] metal surfaces, as well as thin films on metal substrates [54].

ACKNOWLEDGMENTS

This work was supported by the Deutsche Forschungsgemeinschaft (DFG) under Contract No. Wi1336, by the FWF-Austria (Grants No. SFB016-ADLIS, No. SFB041-VICOM, and No. P17359), and the European Union Contract No. HPRI-CT-2005-026015 (Ion Technology and Spectroscopy–Low Energy Ion Beam Facilities). A.S. thanks the International Max Planck Research School–Complex Surfaces in Material Science Ph.D. program of the MPG for financial support. Part of the calculations were performed at the IDRIS supercomputing center, Orsay, France (Project No. 091827). Helpful discussions with J. Vogt (Magdeburg) are gratefully acknowledged.

[1] M. Arndt, O. Nairz, J. Vos-Andreae, C. Keller, G. van der Zouw, and A. Zeilinger, Nature (London) **401**, 680 (1999).
[2] I. Estermann and O. Stern, Z. Phys. **61**, 95 (1930).
[3] D. Farias and K. H. Rieder, Rep. Prog. Phys. **61**, 1575 (1998).
[4] E. Hulpke, ed., *Springer Series in Surface Sciences* (Springer, Berlin, 1992).

[5] A. Schüller, S. Wethekam, and H. Winter, Phys. Rev. Lett. **98**, 016103 (2007).

[6] P. Rousseau, H. Khemliche, A. G. Borisov, and P. Roncin, Phys. Rev. Lett. **98**, 016104 (2007).

[7] A. Schüller and H. Winter, Phys. Rev. Lett. **100**, 097602 (2008).

[8] P. Rousseau, H. Khemliche, N. Bundaleski, P. Soulisse, A. Momeni, and P. Roncin, J. Phys.: Conference Series **133**, 012013 (2008).

[9] H. Winter, Phys. Rep. **367**, 387 (2002).

[10] J. R. Manson, H. Khemliche, and P. Roncin, Phys. Rev. B **78**, 155408 (2008).

[11] F. Aigner, N. Simonović, B. Solleder, L. Wirtz, and J. Burgdörfer, Phys. Rev. Lett. **101**, 253201 (2008).

[12] M. R. Welton-Cook and M. Prutton, Surf. Sci. **74**, 276 (1978).

[13] F. W. de Wette, W. Kress, and U. Schröder, Phys. Rev. B **32**, 4143 (1985).

[14] G. C. Benson and T. A. Claxton, J. Chem. Phys. **48**, 1356 (1968).

[15] G. E. Laramore and A. C. Switendick, Phys. Rev. B **7**, 3615 (1973).

[16] N. Garcia, Phys. Rev. Lett. **37**, 912 (1976).

[17] N. Garcia, J. Chem. Phys. **67**, 897 (1977).

[18] J. G. Roberts, M. A. van Hove, and G. A. Somorjai, Surf. Sci. **518**, 49 (2002).

[19] J. Vogt and H. Weiss, Surf. Sci. **501**, 203 (2002).

[20] Note in Ref. [19] the rumpling is defined as the deviation of the Li^+ and F^- ions from the geometrical mean of the shared layer which differs by a factor of 2 from our definition.

[21] N.-P. Wang, M. Rohlfing, P. Krüger, and J. Pollmann, Phys. Rev. B **67**, 115111 (2003).

[22] A. Schüller, H. Winter, M. S. Gravielle, J. M. Pruneda, and J. E. Miraglia, Phys. Rev. A **80**, 062903 (2009).

[23] J. Vogt, Habilitation thesis, Magdeburg University, 2008 [http://diglib.uni-magdeburg.de/Dissertationen/2008/jocvogt.pdf].

[24] D. S. Gemmell, Rev. Mod. Phys. **46**, 129 (1974).

[25] DLD40, Roentdek Handels GmbH, Kelkheim-Ruppertshain, Germany [http://www.roentdek.com].

[26] U. Garibaldi, A. C. Levi, R. Spadacini, and G. E. Tommei, Surf. Sci. **48**, 649 (1975).

[27] W. F. Avrin and R. P. Merrill, Surf. Sci. **311**, 269 (1994).

[28] A. Schüller and H. Winter, Nucl. Instrum. Methods Phys. Res. B **267**, 628 (2009).

[29] A. W. Kleyn and T. C. M. Horn, Phys. Rep. **199**, 191 (1991).

[30] X. Gonze *et al.*, Comp. Mat. Sci. **25**, 478 (2002).

[31] An alternative to the use of a periodic supercell consists in the use of the embedded cluster approximation where the projectile and a small region of the surface are treated fully quantum mechanically while the surrounding part of the crystal is represented by point charges. This approach was used in our previous calculations [11,55].

[32] N. Troullier and J. L. Martins, Phys. Rev. B **43**, 1993 (1991).

[33] This is because at large distances, the potential curves have an attractive low-energy tail due to the polarization of the He projectile by the surface ions [56]. Convergence of this tail requires large basis sets and a proper inclusion of exchange-correlation effects. Depending on the approximation, the corrugation decreases (Ref. [11]), increases (this work), or remains almost constant (Ref. [22]) with decreasing energy.

[34] S. Baroni, S. de Gironcoli, A. Dal Corso, and P. Giannozzi, Rev. Mod. Phys. **73**, 515 (2001).

[35] X. Gonze, Phys. Rev. B **55**, 10337 (1997); X. Gonze and C. Lee, *ibid.* **55**, 10355 (1997).

[36] The FHI98PP pseudopotential generator was used. M. Fuchs and M. Scheffler, Comput. Phys. Commun. **119**, 67 (1999).

[37] H. Bilz and W. Kress, *Phonon Dispersion Relations in Insulators* (Springer-Verlag, Berlin Heidelberg, 1979).

[38] G. Brusdeylins, R. B. Doak, and J. P. Toennies, Phys. Rev. B **27**, 3662 (1983).

[39] G. Bracco, M. d'Avanco, C. Salvo, R. Tatarek, S. Terreni, and F. Tommasini, Surf. Sci. **189-190**, 684 (1987).

[40] We note, however, an overestimation of the Rayleigh mode frequency around M by about 10%. We assume that this error is due to the local-density approximation which tends to overbind and may thus overestimate the frequencies of vertical vibrations of the outermost layer. A similar overestimation by 11% of the Rayleigh mode frequency (but for a different reason) was observed in calculations of the surface phonons of LiF by the shell model. For more information on this and other aspects of surface phonons, we refer the reader to the review in Ref. [57].

[41] J. P. Perdew and S. Kurth, in *A Primer in Density Functional Theory*, edited by C. Fiolhais, F. Nogueira, and M. A. L. Marques, Springer Lecture Notes in Physics, Vol. 620 (Springer, New York, 2003).

[42] R. K. Gupta, Phys. Rev. B **12**, 4452 (1975).

[43] We performed a fit in terms of a sum over pairwise potentials for the He-Li^+ and He-F^- interactions. The total potential is fitted to our *ab initio* calculation of the potential hypersurface of the unperturbed planar crystal surface. We use the simple form $V(r) = a\exp(-br) - c/r^6$ which gives a fairly good fit of both the He-Li^+ and He-F^- pairwise potentials around the potential minimum and up to 1 eV energy. For He-Li^+, our fit yields $a = 925.7$, $b = 2.61$, $c = 216.15$. For He-F^-, we obtain $a = 1019.0$, $b = 2.23$, $c = 116.70$. Spatial coordinates are in a.u., V in eV.

[44] T. Minami, C. O. Reinhold, and J. Burgdörfer, Phys. Rev. A **67**, 022902 (2003); M. Seliger *et al.*, *ibid.* **75**, 032714 (2007) and references therein.

[45] M. D. Feit and J. A. Fleck Jr., J. Chem. Phys. **78**, 301 (1983); **80**, 2578 (1984).

[46] J. Lienemann, A. Schüller, D. Blauth, J. Seifert, S. Wethekam, M. Busch, K. Maass, and H. Winter, Phys. Rev. (submitted for publication).

[47] L. Wirtz *et al.* (to be published).

[48] H. Khemliche, P. Rousseau, P. Roncin, V. H. Etgens, and F. Finocchi, Appl. Phys. Lett. **95**, 151901 (2009).

[49] A. Momeni, P. Soulisse, P. Rousseau, H. Khemliche, and P. Roncin, e-Journal of Surface Science and Nanotechnology **8**, 101 (2010).

[50] N. Bundaleski, H. Khemliche, P. Soulisse, and P. Roncin, Phys. Rev. Lett. **101**, 177601 (2008).

[51] M. Busch, A. Schüller, S. Wethekam, and H. Winter, Surf. Sci. **603**, L23 (2009).

[52] A. Schüller, M. Busch, S. Wethekam, and H. Winter, Phys. Rev. Lett. **102**, 017602 (2009).
[53] A. Schüller, M. Busch, J. Seifert, S. Wethekam, H. Winter, and K. Gärtner, Phys. Rev. B **79**, 235425 (2009).
[54] J. Seifert, A. Schüller, H. Winter, R. Wlodarczyk, J. Sauer, and M. Sierka, Phys. Rev. B **82**, 035436 (2010).
[55] L. Wirtz, J. Burgdörfer, M. Dallos, T. Müller, and H. Lischka, Phys. Rev. A **68**, 032902 (2003).
[56] M. S. Gravielle and J. E. Miraglia, Phys. Rev. A **78**, 022901 (2008).
[57] G. Benedek and J. P. Toennies, Surf. Sci. **299-300**, 587 (1994).